Advanced Composites and Hybrid Materials (2025) 8:213
https://doi.org/10.1007/s42114-025-01294-1

RESEARCH

Halide perovskite-polymer composite film for bright and stable light-emitting devices

Maoding Cheng[1,2] · Brooke Robinson[2] · Manoj Shah[2] · Emad Omar Badradeen[2] · Araceli Herrera Mondragon[3] · Roberto Gonzalez Rodriguez[3] · Jingbiao Cui[3] · Yuankun Lin[3] · Anupama B. Kaul[4] · Fumiya Watanabe[5] · Grant Wangila[2] · Mansour Mortazavi[2] · Chao Yan[1] · Zhanhu Guo[6] · Qinglong Jiang[2]

Received: 16 July 2024 / Revised: 20 February 2025 / Accepted: 4 March 2025

Abstract
Stability is the primary hindrance for the application of halide perovskite material in light-emitting devices, solar cells, and other devices. In this work, halide perovskite and polymer composite film have been prepared for stable and bright light-emitting devices. Pure-phase Cs_4PbBr_6 crystals have been synthesized, and their photoluminescence (PL) properties and fluorescence lifetimes have been investigated. The Cs_4PbBr_6 crystals exhibited high uniformity but underwent rapid photodegradation under light irradiation. To address this issue, we prepared bright light-emitting devices using composite of Cs_4PbBr_6 crystals and polyethylene oxide (PEO) as the emission layer. The aim was to improve the optical and physical properties of halide perovskites, such as photodegradation and stability. PEO, with its excellent film-forming ability, created a uniform and dense film on the halide perovskite surface, filling microscopic defects and providing a protective barrier. FTIR, morphology, and PL analyses confirmed the protective role of the halide perovskite and polymer composite film. The composite film light-emitting devices demonstrated improved stability and higher PL brightness, with a peak brightness approaching 3×10^8 cd/m^2, which was approximately 75% higher than the pure halide perovskite devices.

Keywords Perovskite · Cs_4PbBr_6 · Luminance · Light-emitting device · Composite film · Polyethylene oxide

1 Introduction

In recent years, halide perovskite materials have attracted widespread attention due to excellent optical and electrical properties, including long free carrier diffusion lengths, high carrier mobility, tunable band gaps, high photoluminescence quantum yields, and solution processability [1–5]. The general formula of halide perovskite material is ABX_3, where A is typically a monovalent organic/inorganic cation, such as formamidinium ion, methylammonium ion, and Cs^+; B is a divalent transition metal cation, commonly including Pb^{2+}, Sn^{2+}, and Cd^{2+}; and X is a halide or pseudohalide ion including Cl^-, Br^-, I^-, and SCN^- [6–10]. ABX_3 halide perovskite crystals belong to the three-dimensional perovskite structure, featuring a continuous network of $[PbBr_6]^{4-}$ octahedra, with A^+ ions filling the gaps between adjacent $[BX_6]^{4-}$ octahedra to form a three-dimensional lattice [11, 12]. Halide perovskites are particularly attractive in light-emitting devices and have achieved a series of advancements over the past decade [13–17]. In 2014, Tan et al. fabricated halide perovskite light-emitting diodes (PeLEDs) with an external quantum

✉ Chao Yan
chaoyan@just.edu.cn

✉ Zhanhu Guo
zhanhu.guo@northumbria.ac.uk

✉ Qinglong Jiang
jiangq@uapb.edu

1 School of Material Science and Engineering, Jiangsu University of Science and Technology, Zhenjiang 212100, Jiangsu, China

2 Department of Chemistry and Physics, University of Arkansas at Pine Bluff, Pine Bluff, AR 71601, USA

3 Department of Physics, University of North Texas, Denton, TX 76203, USA

4 Department of Electrical Engineering, University of North Texas, Denton, TX 76207, USA

5 Center for Integrative Nanotechnology Sciences, University of Arkansas at Little Rock, Little Rock, AR 72204, USA

6 Mechanical and Construction Engineering, Faculty of Engineering and Environment, Northumbria University, Newcastle Upon Tyne NE18, UK

Published online: 20 March 2025

efficiency (EQE) of 0.1%, which highlighted the potential of halide perovskite materials in the optoelectronic field [18]. Li et al. achieved a brightness of 591,197 cd/m^2 at 4.8 V in $CsPbBr_3$ light-emitting diodes without a hole transport layer [19]. Xuan and her team reported ultra-efficient green perovskite LEDs, surpassing the milestone of 30% quantum efficiency. By optimizing charge carrier transport and near-field light distribution, they reduced electron leakage and achieved a high light outcoupling efficiency of 41.82% [20, 21].

However, the bond angles in the three-dimensional halide perovskite structure prevent the quantum confinement of charge carriers, resulting in lower photoluminescence quantum yields [13]. Additionally, 3D halide perovskite ABX_3 has poor chemical and environmental stability [22], being highly susceptible to humidity and light exposure, necessitating optimization for stability to enhance its reliability in practical applications [23–26]. A_4BX_6 structured materials are promising candidates: they belong to the zero-dimensional halide perovskite structure, composed of isolated $[BX_6]^{4-}$ octahedra, each surrounded by Cs^+ ions. This structure gives A_4BX_6 materials high chemical and environmental stability, allowing them to remain stable in air. Although it is more stable under nature environmental conditions than ABX_3, Cs_4PbBr_6 is still prone to degradation under prolonged exposure to moisture and light, which can lead to a decline in photoluminescence performance over time. Additionally, the continuous large-scale production of high-quality Cs_4PbBr_6 remains a challenge due to its sensitivity to environmental variables and precursor quality during the crystallization process. One approach to addressing these challenges is to combine polymers with halide perovskite materials to form composite films. This strategy leverages the complementary properties of polymers and halide perovskites to enhance mechanical stability and improve overall device performance while also enhancing the optoelectronic performance of the devices [27]. Polymers such as polyethylene oxide and polyvinylpyrrolidone (PVP) have been studied for their compatibility with halide perovskite materials, demonstrating enhanced film morphology and improved device stability [28–33].

In this work, we synthesized phase-pure Cs_4PbBr_6 crystals and studied their photoluminescence properties and fluorescence lifetime. The Cs_4PbBr_6 crystals exhibited high uniformity, while they quickly underwent photodegradation under light irradiation. To address this issue, we prepared bright light-emitting devices using Cs_4PbBr_6 crystals and PEO composite as the emission layer. The aim was to improve the optical and physical properties of halide perovskites, such as photodegradation and stability. PEO, with its excellent film-forming ability, can create a uniform and dense film on the halide perovskite surface and provide a protective barrier [34]. FTIR, morphology, and PL analyses confirmed the protective role of the halide perovskite and polymer composite film. The composite film light-emitting devices demonstrated improved stability and higher PL brightness, with a peak brightness approaching 3×10^8 cd/m^2, which is approximately 75% higher than that of pure halide perovskite light-emitting devices.

2 Results and discussion

In this approach, the synthesis of phase-pure Cs_4PbBr_6 perovskite crystals was controlled through a vacuum method to avoid the formation of $CsPbBr_3$ (Fig. S1). CsBr and $PbBr_2$ (1:4) were dissolved in DMSO to form a precursor solution. The solution was drop-cast onto FTO glass and heated under vacuum at 120 °C for 24 h to obtain Cs_4PbBr_6 crystals as illustrated in Fig. 1a. Under the optical microscope (Fig. 1c), Cs_4PbBr_6 crystals displayed well-defined, geometrically regular shapes, indicating a successful crystallization process. As shown in Fig. 1, Cs_4PbBr_6 crystals emitted strong green light under UV light. From the high-resolution transmission electron microscopy (HRTEM) image presented in Fig. 1d, we observed the crystalline structure of Cs_4PbBr_6. The inset shows a magnified view with a clear identification of the (214) lattice planes. The measured lattice spacing of 0.31 nm was consistent across different areas of the sample, demonstrating excellent crystal quality and phase purity. This precise structural information is crucial for the electronic and optical properties of these materials. The synthesis and characterization results confirmed that the vacuum method for synthesizing Cs_4PbBr_6 crystals is effective, producing high-quality crystals with desirable optical properties while avoiding the formation of $CsPbBr_3$. This method can be utilized to prepare pure Cs_4PbBr_6 crystal.

The fluorescence lifetime imaging (FLIM) across the surface of the Cs_4PbBr_6 crystal (Fig. 2a–d) and $CsPbBr_3$ crystal (Fig. 2e–h) was revealed in the analysis. The PL lifetime was measured using a picosecond laser with a wavelength of 409 nm and a Micro Time 200 time-resolved confocal fluorescence microscope. The FLIM in Fig. 2a showed that the Cs_4PbBr_6 surface had a lifetime distribution and lifetime events. Figure 2b displays the fast lifetime histogram of the image in Fig. 2a. The sharp peak centered at 15 ns in Fig. 2b indicates a narrow lifetime distribution, which is critical for achieving consistent photoluminescence properties in practical applications. The inset of Fig. 2b shows the corresponding PL excited by 409 nm together with the laser line itself. The bottom-right region exhibits different intensities (colors) compared to the top-left corner in fluorescence lifetimes in Fig. 2a. It can be argued that it is due to the sample alignment in the experimental setup. A further study revealed that the bottom-right region has a slightly higher lifetime than the top-left corner which is closer to the edge of the crystal

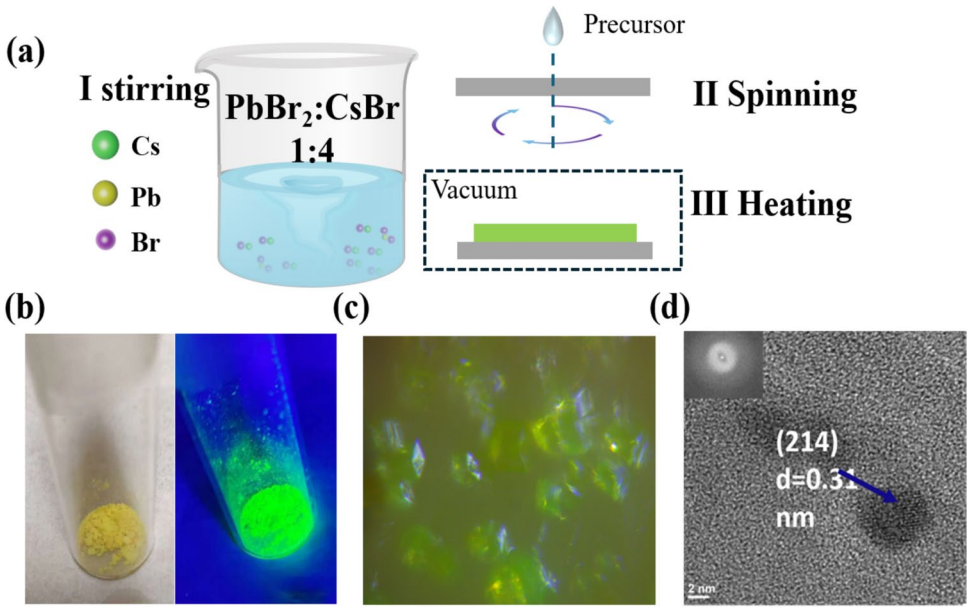

Fig. 1 **a** Synthesis of Cs_4PbBr_6 crystals. **b** Cs_4PbBr_6 crystal powder and under a UV light. **c** Cs_4PbBr_6 crystals under microscope. **d** HRTEM morphology and lattice structure of Cs_4PbBr_6 crystals

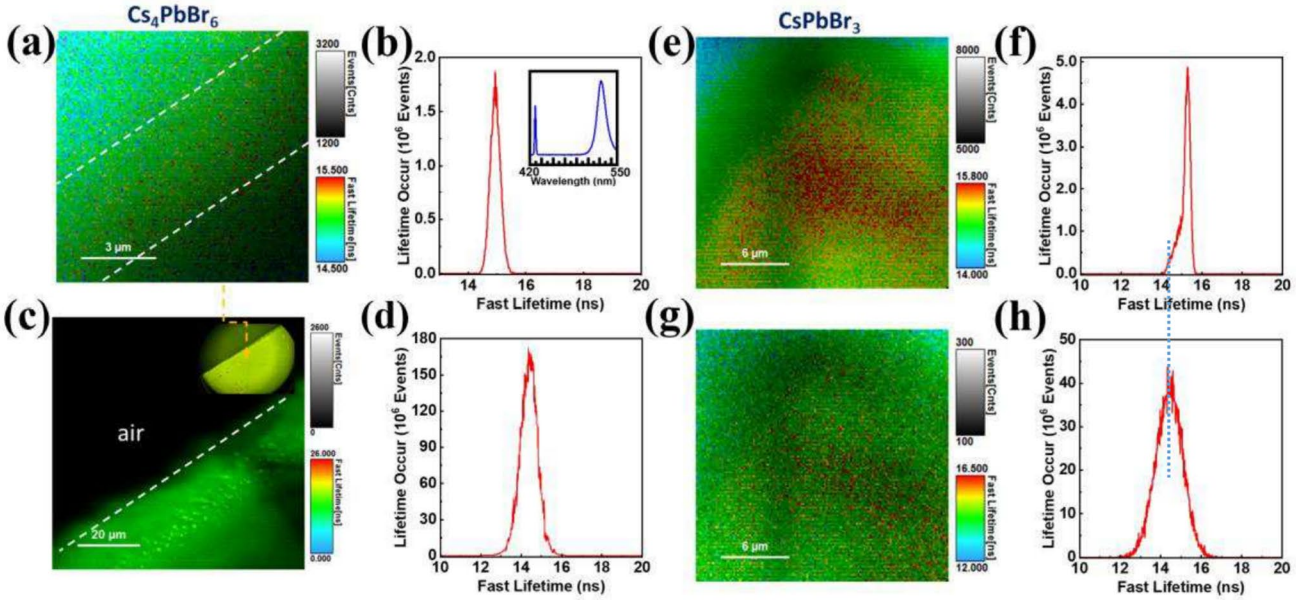

Fig. 2 **a**–**d** The fluorescence lifetime imaging and lifetime histogram of Cs_4PbBr_6 . **e**–**h** $CsPbBr_3$ crystals. FLIM of Cs_4PbBr_6 crystal away from the crystal edge (**a**) and near the edge (**c**) and their corresponding lifetime histogram (**b**, **d**). The inset in b shows the PL excited by 409 nm together with 409 nm laser line. The inset in c is the microscope image of the measured Cs_4PbBr_6 crystal. All dashed white lines are parallel. FLIM of $CsPbBr_3$ crystal on the surface (**e**) and 0.17 mm beneath the surface (**g**) and their corresponding lifetime histogram (**f**–**h**)

as shown in the inset of Fig. 2c. Figure 2a can be divided into three regions by dashed white lines parallel to the crystal edge in Fig. 2c. The FLIM and the lifetime histogram at the edge in Fig. 2c and d has a slightly smaller lifetime (14.5 ns) than the one away from the edge in Fig. 2a and b. It explains the slight intensity (color) distribution along the diagonal direction perpendicular to the dashed white lines. Figure 2e and f shows the fluorescence lifetime imaging and fluorescence lifetime distribution of the $CsPbBr_3$ crystal. The large red areas in the center of Fig. 2e indicate regions with longer fluorescence lifetimes, while the green and blue areas represent shorter lifetimes. Figure 2f shows a broad lifetime distribution below 15 ns for $CsPbBr_3$ crystal. The main peak exhibits a pronounced sharp peak with a clearly defined peak position. There are minor fluctuations at the base of the peak. By focusing the laser 0.17 mm beneath the

sample surface, the measured FLIM in Fig. 2g has less red colors than the one in Fig. 2e, and the lifetime histogram in Fig. 2h reproduces the tail below 15 ns as indicated by the dash line. We can consider the lifetime in Fig. 2h for $CsPbBr_3$ bulk.

The synthesized Cs_4PbBr_6 crystal exhibits a high degree of uniformity in terms of fluorescence lifetime and photoluminescence efficiency, which are essential for the reliable performance of optoelectronic devices utilizing these crystals. These results confirm the effectiveness of our synthesis approach in producing high-quality Cs_4PbBr_6 crystal.

We examined the photoluminescence properties of phase-pure Cs_4PbBr_6 crystals under 2-h exposure to 375 nm UV laser on days 1, 2, and 3 as shown in Fig. 3a. On all days, PL intensity dropped quickly once the crystal was exposed to UV laser for 1 min, dropped fast in 1 h, and then slowly after 1 h. On day one, the PL intensity dropped from 10,100 to 7100 with about 29.7% decrease. The self-healing brought the PL intensity to 9600 after keeping the crystal in dark for overnight. On day two, the PL intensity dropped from 9600 to 6900 with about 28.1% decrease and from 8800 to 6700 with about 23.8% decrease on day three. Figure 3b shows the PL spectra at the end of exposure on day one, two, and three. The PL intensity dropped after each day (33.8% decrease). The PL wavelength did not shift, as indicated by the dashed line. Then, 519 nm PL was observed. The crystal's PL intensity gradually but steadily declines, indicating progressive degradation over time. The PL emission results confirm the Cs_4PbBr_6 crystal's sensitivity to UV light, likely due to changes in exciton recombination processes triggered by UV-induced damage.

The stability of halide perovskites is critical for long-term operation. To enhance the stability, we added 10% wt PEO to the Cs_4PbBr_6 precursor solution, forming a mixed solution (Fig. S2). After stirring evenly, a drop of the solution was spin-coated onto the wick (Fig. S3). The wick was then placed in a vacuum oven and heated for 24 h, resulting in a uniform and dense Cs_4PbBr_6-PEO composite film on the surface of the wick, as shown in Fig. 4a. Firstly, the PEO film exhibited high optical transparency, which did not significantly affect the optical properties of the halide perovskite material. This characteristic is particularly important for optoelectronic applications, as it ensures efficient light transmission and utilization. Secondly, PEO demonstrated excellent film-forming properties, capable of forming a uniform, dense, and smooth film on the wick surface. Figure 4b shows optical and scanning electron microscopy (SEM) images of the Cs_4PbBr_6 film and Cs_4PbBr_6-PEO film on the surface of the wicks. By comparing these images, it can be observed that PEO also helped to disperse the halide perovskite crystals, preventing their grains from becoming too large. Smaller and even halide perovskite grains generally have higher photoluminescence efficiency due to less recombination, while larger grains can cause severe recombination, reduce film uniformity, and lower photoluminescence efficiency [35, 36].

The presence of PEO in the halide perovskite films was confirmed by reflection Fourier-transform infrared (FTIR) spectra. In Fig. 4c, the FTIR spectra provided more insights into the chemical composition and interactions within the composite film. Both the PEO and the halide Cs_4PbBr_6-PEO composite film exhibited C-H stretching vibrations at 2875 cm^{-1} and 1460 cm^{-1} [37, 38]. In contrast, the pure halide perovskite film did not show corresponding infrared characteristic peaks. Additionally, we compared the Raman spectra of Cs_4PbBr_6-PEO composite film, PEO and Cs_4PbBr_6 film (Fig. S4). The PEO spectrum displayed distinct characteristic peaks at 870 cm^{-1}, 1150 cm^{-1}, and 1423 cm^{-1}, corresponding to the symmetric and asymmetric stretching vibrations of C–O–C bonds and CH_2

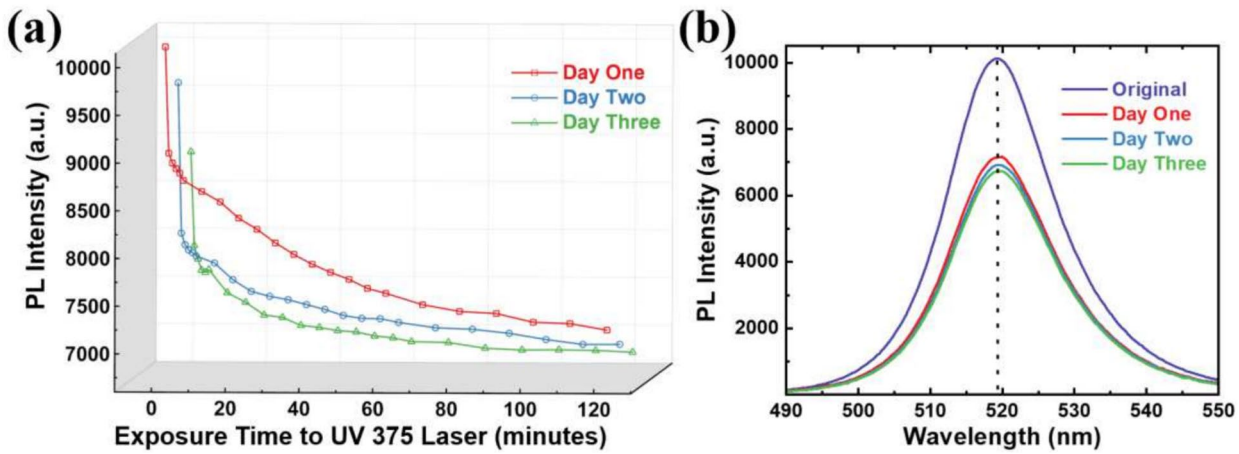

Fig. 3 **a** PL intensity of Cs_4PbBr_6 as a function exposure time to UV 375 nm laser. **b** PL of Cs_4PbBr_6 at the beginning of UV exposure (original) and at the end of days one, two, and three

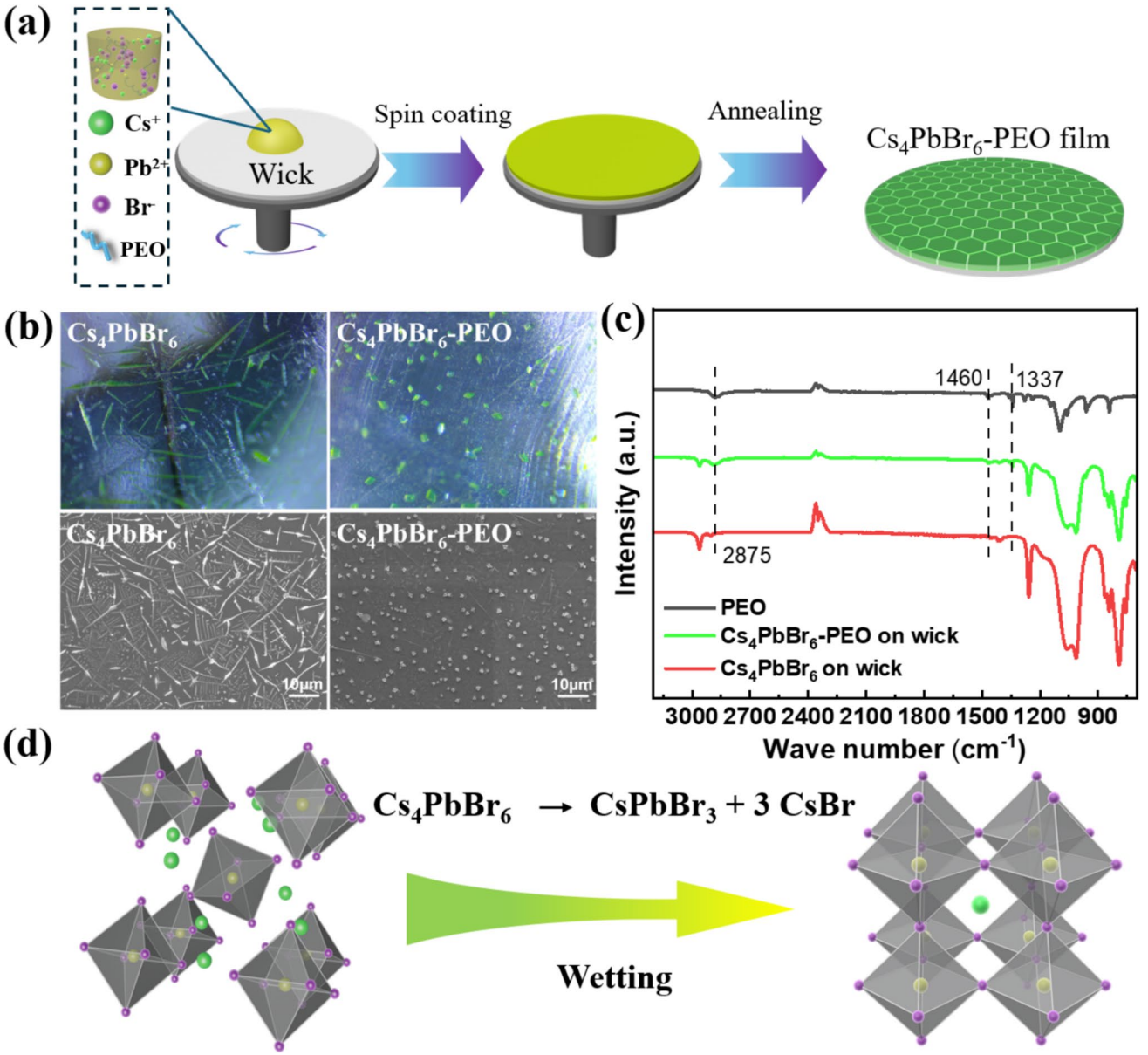

Fig. 4 **a** Synthesis of Cs_4PbBr_6-PEO composite film on wick. **b** SEM images and optical images of Cs_4PbBr_6 film on wick and Cs_4PbBr_6-PEO composite film on wick. **c** FTIR spectra of PEO, Cs_4PbBr_6 film on wick, and Cs_4PbBr_6-PEO composite film on wick. **d** Overview of transformation reactions of Cs_4PbBr_6 nanocrystals into $CsPbBr_3$ nanocrystals

deformation vibrations, respectively [39–41]. There are no peaks for pure Cs_4PbBr_6 above 200 cm^{-1} [42–44]. On this basis, the spectrum of the Cs_4PbBr_6-PEO composite film showed peaks close to those of the PEO spectrum. Although the intensity was lower and slightly shifted, this was due to the interactions between PEO and the perovskite crystals. These spectra confirmed that we successfully synthesized the Cs_4PbBr_6-PEO composite film.

To further verify the purity of the Cs_4PbBr_6 crystal, XRD measurements were conducted for a comprehensive analysis of the composite film and crystal (Fig. S5). The XRD pattern of the sample predominantly matched the characteristic diffraction peaks of Cs_4PbBr_6, indicating that Cs_4PbBr_6 is the primary phase in the material. After the addition of PEO, the main diffraction peaks of Cs_4PbBr_6 remain prominent and show no significant shifts in their positions. This indicates that the crystalline structure of Cs_4PbBr_6 is not significantly affected by the presence of PEO.

As reported in the literature, Cs_4PbBr_6 phases can be converted to $CsPbBr_3$ phases in a humid environment [23, 45, 46]. Figure 4d presents an overview of the transformation of Cs_4PbBr_6 nanocrystals into $CsPbBr_3$ nanocrystals.

Therefore, if a significant portion of Cs_4PbBr_6 crystals were to transform into $CsPbBr_3$ crystals, the brightness of the device would be adversely affected (Fig. S6). We spin-coated Cs_4PbBr_6 film and Cs_4PbBr_6-PEO film onto wicks and placed them in an indoor environment for several days. The surface morphologies were then observed using an optical microscope (Fig. S7). Large green Cs_4PbBr_6 crystals and yellow $CsPbBr_3$ crystals were clearly visible on the pure Cs_4PbBr_6 film. In contrast, no yellow $CsPbBr_3$ crystals were observed on the composite film. Cs_4PbBr_6 is a zero-dimensional perovskite structure and composed of isolated $[PbBr_6]^{4-}$ octahedra separated by Cs^+ ions. In the presence of moisture or water, this structure tends to decompose as water molecules penetrate the lattice, breaking the bonds between octahedra and restructuring to form $CsPbBr_3$ crystals [47, 48].

The green light-emitting device was excited using a wick. The wick used in the study emits violet light with a peak wavelength of 365 nm, and its maximum brightness was measured to be approximately 9×10^7 cd/m^2. After spin-coating the Cs_4PbBr_6-PEO composite film onto the wick, the device emitted green light with increased brightness, indicating that the significant increase in brightness is attributed to the light emitting of the composite film. The emission spectrum of the wick was measured and confirmed to exhibit a peak at 365 nm (Fig. S8a). The luminance versus voltage characteristics of the device are shown in Fig. S6, demonstrating the enhanced brightness due to the Cs_4PbBr_6 composite film. Furthermore, the current efficiency of the wick is provided in Fig. S8b. As shown in Fig. 5a, all halide perovskite light-emitting devices exhibited higher brightness than the devices using the wick alone. The pure halide perovskite light-emitting devices reached a maximum brightness of 1.6×10^8 cd/m^2 at 3.4 V. After UV light is absorbed by Cs_4PbBr_6, electrons transited to a higher energy level and then quickly return to a lower energy level and emitting green light with a longer wavelength (lower energy). This energy conversion (Stokes shift) helps improve the efficiency of visible light emission. The Cs_4PbBr_6-PEO composite film light-emitting devices reached a maximum brightness of 2.8×10^8 cd/m^2 at 3.5 V with a current efficiency of 30 cd/A (Fig. 5b). The brightness of the pure Cs_4PbBr_6 light-emitting devices was lower than that of the Cs_4PbBr_6-PEO composite film light-emitting devices, partly because some Cs_4PbBr_6 reacted with moisture in

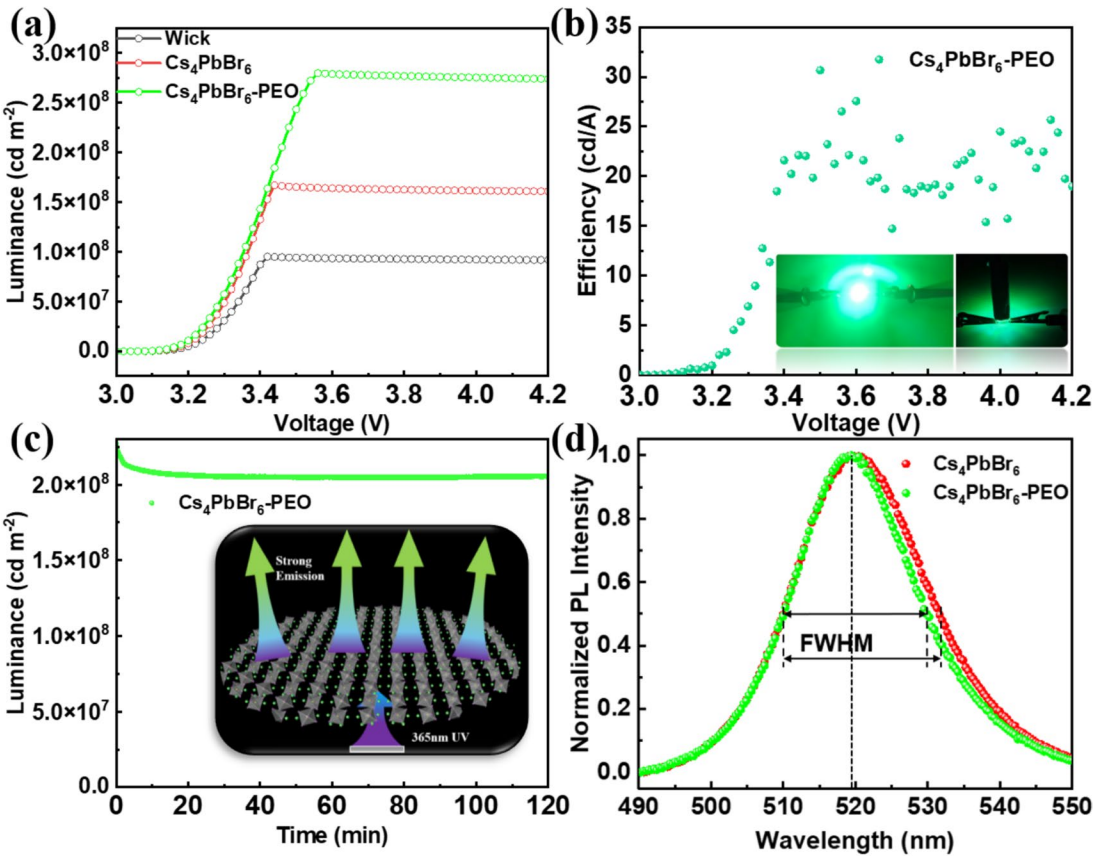

Fig. 5 Green light-emitting device: **a** luminance vs. voltage characteristics of the light-emitting device. **b** Current efficiency. **c** Luminance stability of Cs_4PbBr_6-PEO composite film light-emitting device over time and the PL emission process. **d** PL spectra

the air, converting to $CsPbBr_3$ and CsBr. $CsPbBr_3$ produces very low light response under illumination [49]. The luminescent properties of corresponding devices based on $CsPbBr_3$ are shown in Fig. S6, which indicates that $CsPbBr_3$ crystals are not a good candidate for this case. Another reason is that PEO significantly improved the optical properties of Cs_4PbBr_6 crystals by reducing defects and enhancing crystal quality, thereby increasing PL efficiency [50]. To verify the reasonableness of using 10% wt PEO, we tested Cs_4PbBr_6-PEO composite film devices with different ratios ranging from 5 to 25% (Fig. S9). Among them, the 10% wt perovskite-PEO devices exhibited the highest brightness. Although the 25% wt Cs_4PbBr_6-PEO composite film light-emitting device had higher brightness than the 20% Cs_4PbBr_6-PEO composite film light-emitting device, further increasing the PEO ratio would lead to phase separation between the halide perovskite and PEO, forming an uneven composite film (Fig. S10). Additionally, compared to other polymers with good film-forming properties and light transmittance, such as PMMA and PVP, PEO still demonstrated superior brightness (Fig. S11).

To further test the stability of the halide perovskite and polymer composite film, the Cs_4PbBr_6-PEO light-emitting device was operated continuously at 3.5 V for 2 h. The device's brightness slightly decayed in the first few minutes and then maintained a very stable level, as shown in Fig. 5c. The initial decay in brightness may be related to the wick heating up, leading to increased resistance of wick.

The solid-state photoluminescence spectra of the pure light-emitting devices and Cs_4PbBr_6-PEO composite film light-emitting devices are shown in Fig. 5d. Both the pure and Cs_4PbBr_6-PEO composite film light-emitting devices exhibit emission peaks at 519 nm, which is close to the reported PL peak of Cs_4PbBr_6 [13, 49, 51]. Notably, the PL peak of the Cs_4PbBr_6-PEO composite film light-emitting device has a full width at half maximum (FWHM) of approximately 20.0 nm, which is 1.8 nm narrower than the pure Cs_4PbBr_6. This result indicates a more uniform emission center, which results in a more concentrated emission spectrum. This is primarily because the presence of PEO helps control the crystal growth, leading to a more uniform particle size distribution. These results demonstrate that incorporating PEO into light-emitting devices not only enhances brightness and efficiency but also significantly improves stability and reduces degradation under continuous operation. In recent years, the developments of more sophisticated materials for electric-optoelectronic devices have been a hot topic for scientific inquiry and technical advancement [52]. These results make the Cs_4PbBr_6-PEO composite film a promising material for high-performance optoelectronic applications.

3 Conclusions

In this study, we successfully synthesized phase-pure Cs_4PbBr_6 crystals and developed Cs_4PbBr_6-PEO composite films to enhance the performance and stability of light-emitting devices. The synthesis method employed, involving a vacuum process, yielded Cs_4PbBr_6 crystals with high uniformity and well-defined geometrical shapes. The photoluminescence properties of these crystals demonstrated high uniformity in electronic states, as evidenced by consistent fluorescence lifetimes. To address the issue of photodegradation and enhance the stability of the halide perovskite material, we incorporated 10% wt PEO into the Cs_4PbBr_6 precursor solution. The resulting Cs_4PbBr_6-PEO composite film exhibited high optical transparency and excellent film-forming properties, creating a uniform, dense, and smooth protective layer on the halide perovskite surface. This composite film effectively dispersed the halide perovskite crystals, preventing excessive grain growth and reducing surface defects, which in turn improved photoluminescence efficiency. Experimental results showed that the Cs_4PbBr_6-PEO light-emitting device had superior environmental stability compared to pure Cs_4PbBr_6 light-emitting device. The composite film prevented significant morphological changes under indoor environmental conditions and maintained high luminance and efficiency during continuous operation. The incorporation of PEO not only enhanced the optical properties of Cs_4PbBr_6 crystals but also improved carrier recombination efficiency and altered the energy distribution of photoluminescence, as indicated by the red shift in the emission peak. Raman spectroscopy and FTIR analyses confirmed the successful integration of PEO into the halide perovskite structure, providing additional insights into the chemical composition and interactions within the composite film. In summary, the Cs_4PbBr_6-PEO composite film demonstrated significant improvements in brightness, efficiency, and stability, making it a promising material for high-performance optoelectronic applications. These findings highlight the potential of polymer-assisted crystallization in advancing halide perovskite-based devices and pave the way for future developments in this field.

Supplementary Information The online version contains supplementary material available at https://doi.org/10.1007/s42114-025-01294-1.

Acknowledgements We thank Dr. Jeffery L. Coffer Texas Christian University for using his TEM.

Author contribution M.C. and B.R. did the synthesis. M.C. made the device and did the light emitting measurements. M.S. did the Raman. A.H., M.G.R, J.C. and Y.L. did the PL measurements. F.W. did the electron microscope. E.B. did the XRD. M.C., Q.J., Z. G, A.B.K, G.W., M.M. and C.Y. did the writing and revising. Q.J. designed the research.

Funding This research was funded by the U.S. DOE/NNSA (award number DE-NA0004114). This project was funded in part by NSF Award # 2228891, 2329842, 2011901, and 2128367.

This research was prepared as an account of work sponsored by an agency of the United States Government. Neither the United States Government nor any agency thereof, nor any of their employees, makes any warranty, express or implied, or assumes any legal liability or responsibility for the accuracy, completeness, or usefulness of any information, apparatus, product, or process disclosed, or represents that its use would not infringe privately owned rights. Reference herein to any specific commercial product, process, or service by trade name, trademark, manufacturer, or otherwise does not necessarily constitute or imply its endorsement, recommendation, or favoring by the United States Government or any agency thereof. The views and opinions of authors expressed herein do not necessarily state or reflect those of the United States Government or any agency thereof.

Data availability No datasets were generated or analysed during the current study.

Declarations

Competing interests The authors declare no competing interests.

References

1. Wang W, Li J, Ni P, Liu B, Chen Q, Lu Y, Wu H, Cao B, Liu Z (2019) Improved synthesis of perovskite $CsPbX_3@SiO_2$ (X = Cl, Br, and I) quantum dots with enhanced stability and excellent optical properties. ES Mater Manuf 4:66–73
2. Jiang Q, Sheng X, Li Y, Feng X, Xu T (2014) Rutile TiO_2 nanowire-based perovskite solar cells. Chem Commun 50(94):14720–14723
3. Zhang P, Wu S, Chen Y, Li X, Sun F, Liu M, Chen Z, Li S (2022) Hysteresis-free and efficient perovskite solar cells using SnO_2 with self-assembly L-cysteine layer. Eng Sci 20:180–187
4. Saparov B, Mitzi D B (2016) Organic–inorganic perovskites: structural versatility for functional materials design. Chem Rev 116(7):4558–4596
5. Jiang Q, Zeng X, Wang N, Xiao Z, Guo Z, Lu J (2018) Electrochemical lithium doping induced property changes in halide perovskite $CsPbBr_3$ crystal. ACS Energy Lett 3(1):264–269
6. Vighnesh K, Wang S, Liu H, Rogach AL (2022) Hot-injection synthesis protocol for green-emitting cesium lead bromide perovskite nanocrystals. ACS Nano 16(12):19618–19625
7. Yu R, Li C, Zhao B, Tan Z, a, (2024) Frontiers in green perovskite light-emitting diodes. Laser Photonics Rev 18(4):2300780
8. Shang Y, Liao Y, Wei Q, Wang Z, Xiang B, Ke Y, Liu W, Ning Z (2019) Highly stable hybrid perovskite light-emitting diodes based on Dion-Jacobson structure. Sci Adv 5(8):eaaw8072
9. Wang Y, Wu T, Barbaud J, Kong W, Cui D, Chen H, Yang X, Han L (2019) Stabilizing heterostructures of soft perovskite semiconductors. Science 365(6454):687–691
10. Jiang Q, Rebollar D, Gong J, Piacentino EL, Zheng C, Xu T (2015) Pseudohalide-induced moisture tolerance in perovskite $CH_3NH_3Pb(SCN)_2I$ thin films. Angew Chem Int Ed 54(26):7617–7620
11. Shi D, Adinolfi V, Comin R, Yuan M, Alarousu E, Buin A, Chen Y, Hoogland S, Rothenberger A, Katsiev K, Losovyj Y, Zhang X, Dowben PA, Mohammed OF, Sargent EH, Bakr OM (2015) Low trap-state density and long carrier diffusion in organolead trihalide perovskite single crystals. Science 347(6221):519–522
12. Green MA, Ho-Baillie A, Snaith HJ (2014) The emergence of perovskite solar cells. Nat Photonics 8(7):506–514
13. Jiang J, Wang D, Wu M, Peng P, Li F-F, Liu F, Jing R, Ma X, Chao Y, Xiao Z, Jiang Q (2020) Ultrasonication-assisted trace amount solvent synthesis of Cs_4PbBr_6 crystal with ultra-bright green light emission. APL Mater 8(7):071115
14. Jiang Q, Chen M, Li J, Wang M, Zeng X, Besara T, Lu J, Xin Y, Shan X, Pan B, Wang C, Lin S, Siegrist T, Xiao Q, Yu Z (2017) Electrochemical doping of halide perovskites with ion intercalation. ACS Nano 11(1):1073–1079
15. Torchyniuk PV, V'yunov OI, Ishchenko AA, Kurdyukova IV, Belous AG (2022) Synthesis of organic-inorganic perovskite $CH_3NH_3PbI_3$ using dimethyl sulfoxide (DMSO) solvent. Eng Sci 17:156–166
16. Sadullah M, Ghosh K (2023) Low-temperature deposition of perovskite $CH_3NH_3PbX_3$ (X = I, Br) thin films using aerosol assisted CVD via vertical flow for photovoltaic applications. ES Energy Environ 20:883
17. Jiang J, Xu J, Walter H, Kazi A, Wang D, Wangila G, Mortazavi M, Yan C, Jiang Q (2020) The doping of alkali metal for halide perovskites. ES Mater Manuf 7:25–33
18. Tan Z-K, Moghaddam RS, Lai ML, Docampo P, Higler R, Deschler F, Price M, Sadhanala A, Pazos LM, Credgington D, Hanusch F, Bein T, Snaith HJ, Friend RH (2014) Bright light-emitting diodes based on organometal halide perovskite. Nat Nanotechnol 9(9):687–692
19. Li J, Shan X, Bade SGR, Geske T, Jiang Q, Yang X, Yu Z (2016) Single-layer halide perovskite light-emitting diodes with sub-band gap turn-on voltage and high brightness. J Phys Chem Lett 7(20):4059–4066
20. Bai W, Xuan T, Zhao H, Dong H, Cheng X, Wang L, Xie R-J (2023) Perovskite light-emitting diodes with an external quantum efficiency exceeding 30%. Adv Mater 35(39):2302283
21. Cheng M, Jiang J, Yan C, Lin Y, Mortazavi M, Kaul AB, Jiang Q (2024) Progress and application of halide perovskite materials for solar cells and light emitting devices. Nanomaterials 14(5):391
22. Zhuang J, Wang J, Yan F (2023) Review on chemical stability of lead halide perovskite solar cells. Nanomicro Lett 15(1):84 13
23. Wang Z, Zhang Y, Liu X, Yu Y, Xu F, Ding J, Liang X, Yang K, Xiang W (2021) High stability and strong luminescence $CsPbBr_3$/Cs_4PbBr_6 perovskite nanocomposite: large-scale synthesis, reversible luminescence, and anti-counterfeiting application. Adv Mater Technol 6(12):2100654
24. Padilla C, Aryal S, Sumant A, Jiang Q, Kaul A B (2023) Comparative analysis of white-light absorption efficiency in multi-dimensional perovskites. 2023 IEEE MetroCon pp: 1–3
25. Tang J, Wu S, AlMasoud N, Alomar TS, Wasnik P, Li H, El-Bahy ZM, Ren J, Li X, Zhang P, Li S, Jiang Q (2023) Defect

passivation in perovskite films by p-methoxy phenylacetonitrile for improved device efficiency and stability. Adv Compos Hybrid Mater 6(5):155
26. Rokade A, Tarkas H, Rokade A, Waman V, Upasani D, Sali JV, Jadkar SR (2023) Effect of incorporation of SnS nanorods on the growth mechanism, crystallinity, optoelectronic performance, and stability of $CH_3NH_3PbI_3$ perovskite active layer. ES Mater Manuf 22:937
27. Qian F, Jia R, Cheng M, Chaudhary A, Melhi S, Mekkey SD, Zhu N, Wang C, Razak F, Xu X, Yan C, Bao X, Jiang Q, Wang J, Hu M (2024) An overview of polylactic acid (PLA) nanocomposites for sensors. Adv Compos Hybrid Mater 7(3):75
28. Huisman BAH, Bolink HJ (2023) Polymer-encapsulated halide perovskite color converters. Adv Opt Mater 11(16):2202921
29. Li J, Bade SGR, Shan X, Yu Z (2015) Single-layer light-emitting diodes using organometal halide perovskite/poly(ethylene oxide) composite thin films. Adv Mater 27(35):5196–5202
30. Gu Z, Wang Y, Wang S, Zhang T, Zhao R, Hu X, Huang Z, Su M, Xu Q, Li L, Zhang Y, Song Y (2022) Controllable printing of large-scale compact perovskite films for flexible photodetectors. Nano Res 15(2):1547–1553
31. Niu Y, He D, Zhang Z, Zhu J, Gavin T, Falaras P, Hu L (2022) Improved crystallinity and self-healing effects in perovskite solar cells via functional incorporation of polyvinylpyrrolidone. J Energy Chem 68:12–18
32. Xiong H, DeLuca G, Rui Y, Zhang B, Li Y, Zhang Q, Wang H, Reichmanis E (2018) Modifying perovskite films with polyvinylpyrrolidone for ambient-air-stable highly bendable solar cells. ACS Appl Mater Interfaces 10(41):35385–35394
33. Zai H, Zhu C, Xie H, Zhao Y, Shi C, Chen Z, Ke X, Sui M, Chen C, Hu J, Zhang Q, Gao Y, Zhou H, Li Y, Chen Q (2018) Congeneric incorporation of $CsPbBr_3$ nanocrystals in a hybrid perovskite heterojunction for photovoltaic efficiency enhancement. ACS Energy Lett 3(1):30–38
34. Nguyen HM, Mader AV, De S, Vapaavuori J (2021) Understanding nanodomain morphology formation in dip-coated PS-b-PEO thin films. Nanoscale Adv 3(17):4996–5007
35. Kumar G, Lin C-C, Kuo H-C, Chen F-C (2024) Enhancing photoluminescence performance of perovskite quantum dots with plasmonic nanoparticles: insights into mechanisms and light-emitting applications. Nanoscale Adv 6(3):782–791
36. Ding H, Shan Y, Wang J, Xu Q, Han J, Jiao M, Cao K, Liu M, Mu H, Zhang S, Yang C (2021) Revealing photoluminescence mechanisms of single $CsPbBr_3/Cs_4PbBr_6$ core/shell perovskite nanocrystals. RSC Adv 11(48):30465–30471
37. Noor SAM, Ahmad A, Talib IA, Rahman MYA (2010) Morphology, chemical interaction, and conductivity of a PEO-ENR50 based on solid polymer electrolyte. Ionics 16(2):161–170
38. Hu P, Han N, Zhang X, Yao M, Cao Y, Zuo A, Yang G, Yuan F (2011) Fabrication of ZnO nanorod-assembled multishelled hollow spheres and enhanced performance in gas sensor. J Mater Chem 21(37):14277–14284
39. Elashmawi IS, H. Gaabour L, (2015) Raman, morphology and electrical behavior of nanocomposites based on PEO/PVDF with multi-walled carbon nanotubes. Results Phys 5:105–110
40. Tong Y, Lin Y, Wang S, Song M (2015) A study of crystallisation of poly (ethylene oxide) and polypropylene on graphene surface. Polymer 73:52–61
41. Naveen Kumar K, Saijyothi K, Vijayalakshmi L, Kang M (2017) Copper–constantan nanoparticles impregnated PEO + PVP:Li^+ blended solid polymer electrolyte films for lithium battery applications. Polym Bull 74(7):2545–2564
42. Qin Z, Dai S, Hadjiev VG, Wang C, Xie L, Ni Y, Wu C, Yang G, Chen S, Deng L, Yu Q, Feng G, Wang ZM, Bao J (2019) Revealing the origin of luminescence center in 0D Cs_4PbBr_6 perovskite. Chem Mater 31(21):9098–9104
43. Zeng W, Liu X, Guo X, Niu Q, Yi J, Xia R, Min Y (2017) Morphology analysis and optimization: crucial factor determining the performance of perovskite solar cells. Molecules 22(4):520
44. Ma Z, Liu Z, Lu S, Wang L, Feng X, Yang D, Wang K, Xiao G, Zhang L, Redfern SAT, Zou B (2018) Pressure-induced emission of cesium lead halide perovskite nanocrystals. Nat Commun 9(1):4506
45. Palazon F, Almeida G, Akkerman QA, De Trizio L, Dang Z, Prato M, Manna L (2017) Changing the dimensionality of cesium lead bromide nanocrystals by reversible postsynthesis transformations with amines. Chem Mater 29(10):4167–4171
46. Cha J-H, Han JH, Yin W, Park C, Park Y, Ahn TK, Cho JH, Jung D-Y (2017) Photoresponse of $CsPbBr_3$ and Cs_4PbBr_6 perovskite single crystals. J Phys Chem Lett 8(3):565–570
47. Cottingham P, Brutchey RL (2016) Compositionally dependent phase identity of colloidal $CsPbBr_{3-x}I_x$ quantum dots. Chem Mater 28(21):7574–7577
48. Maji P, Sadhukhan P, Das S (2020) Optoelectronic properties of facile synthesized orthorhombic cesium lead bromide ($CsPbBr_3$). J Mater Sci: Mater Electron 31(19):17100–17109
49. Saidaminov MI, Almutlaq J, Sarmah S, Dursun I, Zhumekenov AA, Begum R, Pan J, Cho N, Mohammed OF, Bakr OM (2016) Pure Cs_4PbBr_6: highly luminescent zero-dimensional perovskite solids. ACS Energy Lett 1(4):840–845
50. Han T-H, Lee J-W, Choi C, Tan S, Lee C, Zhao Y, Dai Z, De Marco N, Lee S-J, Bae S-H, Yuan Y, Lee HM, Huang Y, Yang Y (2019) Perovskite-polymer composite cross-linker approach for highly-stable and efficient perovskite solar cells. Nat Commun 10(1):520
51. Rakita Y, Kedem N, Gupta S, Sadhanala A, Kalchenko V, Böhm ML, Kulbak M, Friend RH, Cahen D, Hodes G (2016) Low-temperature solution-grown $CsPbBr_3$ single crystals and their characterization. Cryst Growth Des 16(10):5717–5725
52. Das HS, Das DK, Maity SK, Khatua D, Gupta GK, Jalgham R, Akitsu T, Kaushik A, Bhattacharyya S, Roymahapatra G (2024) Analysis of the influence of the thickness of transparent conducting oxide (GZO) with Ga-doping and its use as anode materials in organic light-emitting diodes. ES Energy & Environment 25:1239